Imaging Fast Calcium Currents beyond the Limitations of Electrode Techniques

Nadia Jaafari, Michel de Waard, Marco Canepari

Biophysical Journal, in press

Imaging Fast Calcium Currents beyond the Limitations of Electrode Techniques

Nadia Jaafari[1,2,3], Michel De Waard[1,3] and Marco Canepari[1,2,3]

[1] Inserm U836, Grenoble Institute of Neuroscience, Team 3, Grenoble Cedex 09, France
[2] Université Joseph Fourier, Laboratoire Interdisciplinare de Physique (CNRS UMR 5588), France
[3] Laboratories of Excellence, Ion Channel Science and Therapeutics

Corresponding author: Marco Canepari, INSERM U836 - Grenoble Institute of Neuroscience, Bâtiment Edmond Safra, Chemin F. Ferrini, Site santé de la Tronche - BP 170, 38042 Grenoble cedex 9, France. Email: marco.canepari@ujf-grenoble.fr

Running title: Imaging fast calcium currents

Keywords: Calcium imaging; Voltage imaging; voltage-gated calcium channels, neuronal dendrites.

ABSTRACT

The present understanding of Ca^{2+} channel function is derived from the use of the patch clamp technique. In particular, the measurement of fast cellular Ca^{2+} currents is routinely achieved using whole-cell voltage clamp recordings. This experimental approach, however, is not applicable to the study of local native Ca^{2+} channels during physiological changes of membrane potential in complex cells, since the voltage clamp configuration constrains the membrane potential to a given value. Here, we report for the first time that Ca^{2+} currents from individual cells can be quantitatively measured beyond the limitations of the voltage clamp approach using fast Ca^{2+} imaging with low-affinity indicators. The optical measurement of the Ca^{2+} current was correlated with the membrane potential, simultaneously measured with a voltage-sensitive dye to investigate the activation of Ca^{2+} channels along the apical dendrite of the CA1 hippocampal pyramidal neuron during the back-propagation of an action potential. To validate the method, we analysed the voltage-dependence of high- and low-voltage gated Ca^{2+} channels. In particular, we measured the Ca^{2+} current component mediated by T-type channels and we investigated the mechanisms of recovery from inactivation of these channels. This method is expected to become a reference approach to investigate Ca^{2+} channels in their native physiological environment.

INTRODUCTION

The measurement of ionic currents in single-electrode or two-electrode voltage clamp implies that the cell is maintained at a given membrane potential (V_m) by compensating the cell current (1). The current measured with the electrode is the summation of the filtered currents from all different cellular regions, including remote regions where V_m is unclamped (2). To study the function of native channels, including those expressed under pathological conditions, ionic currents should be recorded at the site of origin during physiological changes of V_m. Local current measurements from a limited number of cellular sites can be obtained using dendritic patch clamp recordings with one (3) or two electrodes at the same site (2), but even if the V_m is dynamically clamped locally, this will never correspond to a physiological V_m change occurring in the cell. The limitation of the voltage clamp approach, for a Ca^{2+} current (I_{Ca}), may in principle be overcome by an independent optical measurement of the current at the locus of its origin using fluorescence Ca^{2+} indicators. In an important reference study (4), Kao and Tsien proposed that, in the presence of an endogenous cellular Ca^{2+} buffer, the relaxation time of the dye-Ca^{2+} binding reaction (τ_R) can be approximated by the equation:

$$\tau_R = \frac{1}{K_{ON}^{Dye} \cdot [Ca^{2+}] + K_{OFF}^{Dye}} \quad (1)$$

where K_{ON}^{Dye} and K_{OFF}^{Dye} are the association and dissociation constants of the reaction, respectively. In general, for Ca^{2+} indicators, the association constant is fast and limited by diffusion between $2 \cdot 10^8$ $M^{-1}s^{-1}$ and $6 \cdot 10^8$ $M^{-1}s^{-1}$. The equilibration time of the reaction is therefore mainly determined by the dissociation constant, i.e. by the equilibrium constant (K_D) that varies from indicator to indicator, determining the affinity to Ca^{2+} (4). As shown in Fig. S1 in the Supporting Material, this relaxation time is less than 1 ms for low affinity indicators with K_D > 10 µM, suggesting the possibility of using these indicators for the measurement of a fast I_{Ca}.

In Ca^{2+} imaging recordings, the fractional change of fluorescence ($\Delta F/F_0$) is proportional to the change of Ca^{2+} ions bound to the indicator ($[DCa^{2+}]$) (5). If $[DCa^{2+}]$ is also proportional to the total free Ca^{2+} concentration entering the cell through the plasma membrane ($[Ca^{2+}]_{TOT}$), then I_{Ca} at its site of origin can be in theory extrapolated by the derivative of $\Delta F/F_0$ ($d\Delta F/F_0/dt$). This scenario may occur if the equilibration of the dye-Ca^{2+} binding reaction is faster than the rise time of I_{Ca}, which is possible, in principle, with low-affinity indicators (6). The possibility to measure I_{Ca} optically was theoretically explored by Sabatini and Regehr (7). In that study, a fast Ca^{2+}-$\Delta F/F_0$ measurement from multiple axons was converted into an optical measurement of I_{Ca}, but without an experimental validation, which requires single-cell resolution and the combined possibility to record the current with an electrode. This validation is crucial since the possibility to extract I_{Ca} from the Ca^{2+}-$\Delta F/F_0$ signal requires two additional conditions. First, the Ca^{2+} bound to the indicator must be proportional to the Ca^{2+} bound to the cell native buffers during the whole Ca^{2+} influx process; in particular, Ca^{2+} sequestration by slow endogenous buffers must be negligible during the current since these mechanisms would decrease $\Delta F/F_0$ independently of $[Ca^{2+}]_{TOT}$. Second, Ca^{2+} release from internal stores should be negligible during the current.

Here, we addressed this challenge using novel technology and we demonstrate experimentally the possibility to record calcium currents (I_{Ca}) by Ca^{2+} imaging experiments, achieving these measurements from distinct subcellular regions of individual neurons. In particular, we measured fast I_{Ca} volume densities mediated by voltage-gated Ca^{2+} channels during physiological changes of V_m, using the low-affinity indicator Oregon Green 488 BAPTA-5N (8,9). The optical measurement of the I_{Ca} was also correlated with V_m, which was simultaneously measured with the intracellularly loaded voltage-sensitive dye JPW1114 (10) allowing exploration of voltage-dependence properties of native Ca^{2+} channels.

MATERIALS AND METHODS

Slice preparation, solutions and electrophysiology

Experiments were approved by the Isere prefecture (Authorisation n. 38 12 01) and the specific protocol (n. 197) by the ethics committee of the Grenoble Institute of Neuroscience. As previously described (11), hippocampal slices (250 µm thick) were prepared from 21-35 postnatal days old C57Bl6 mice using a VF-200 compresstome (Precisionary Instruments, Greenville, NC). Slices were cut in iced extracellular solution and incubated at 37°C for 1 hr before use. The extracellular solution used contained (in mM): 125 NaCl, 26 $NaHCO_3$, 20 glucose, 3 KCl, 1 NaH_2PO_4 and 2 $CaCl_2$ bubbled with 95% O_2 and 5% CO_2. The intracellullar solution contained (in mM): 125 $KMeSO_4$, 5 KCl, 8 $MgSO_4$, 5 Na_2-ATP, 0.3 Tris-GTP, 12 Tris-Phosphocreatine, 20 HEPES, adjusted to pH 7.35 with KOH. To block Na^+ and K^+ channels in voltage clamp experiments, the external solution also contained 1 µM tetrodotoxin, 5 mM tetraethylammonium (TEA), 4 mM 4-aminopyridine and 250 nM apamin, and the internal solution also contained 5 mM TEA. Ca^{2+} indicators were added at the concentration of 1 mM. In voltage-imaging experiments, cells were loaded as previously described (12) with the voltage-sensitive dye JPW1114 dye that was present in the patch pipette at a concentration of 120 µg/mL. In experiments with BAPTA, the internal solution also contained 300 µM EGTA, to prevent a possible decrease of the basal free BAPTA concentration. In experiments with NP-EGTA, the internal solution also contained 150 µM $CaCl_2$ to begin with a free Ca2+ concentration equal to the K_D of NP-EGTA. Indicators and chelators were purchased from Invitrogen (Carlsbad, CA). All other chemicals were purchased either from Tocris (Bristol, UK) or Sigma-Aldrich (St. Louis, MO). Experiments were performed at 32°C using an Olympus BX51 microscope equipped with a 60X/1.0 NA Nikon objective. Patch-clamp recordings were made using a Multiclamp amplifier 700A (Molecular Devices, Sunnyvale, CA) and voltage and current signals were acquired with the A/D board of the CCD camera. The V_m measured with the patch pipette was corrected for the junction potential (-11 mV) as previously estimated (13). In voltage clamp recordings, I_{Ca} was evoked by depolarising pulses from -70 mV to -10 mV and measured in the soma by subtracting the scaled subthreshold current associated with a voltage step from -70 mV to -10 mV.

The imaging system

Simultaneous UV/blue LED illumination from the epifluorescence port of the microscope was allowed by a 409 nm dichroic mirror (FF409, Semrock, Rochester, New York). The 365 nm LED used for photolysis was controlled by an OptoFlash (CAIRN Research Ltd., Faversham, UK) and the 470 nm other LED used for fluorescence excitation was controlled by an OptoLED (also from Cairn). The demagnification of the image and the separation of the two emission wavelengths were done with a previously described system (14). The two images were acquired with a dual-head NeuroCCD-SMQ camera (RedShirtimaging, Decatur, GA) at 510 ± 42 nm (for Ca^{2+}) and at >610 nm (for V_m). The demagnifications of the two aligned images were 0.5X, 0.25X and 0.125X. At 0.125X, it was not possible to obtain the same focal plane for the two images, thus this configuration was used only for individual Ca^{2+} imaging. Although the camera has 80X80 pixels per head (full resolution), to achieve the speed of 20 kHz, binned stripes of 26 × 4 pixels were imaged. In contrast to previous reports (13,15), JPW1114 was excited at 470 nm and not at 532 nm, since this wavelength corresponds to the peak of OG5N emission. The sensitivity of the voltage-sensitive dye at 470 nm was about 4 times less than that at 532 nm. In neurons loaded with only one indicator, either OG5N or JPW1114, the signals detected by the CCD-head devoted to the recording of fluorescence from the other indicator were negligible. Thus, it was possible to unambiguously discriminate Ca^{2+} fluorescence from V_m fluorescence.

Recording and analysis of Ca^{2+} and V_m optical signals

Ca^{2+} recordings, were performed at 20 kHz, starting 20-25 minutes after establishing the whole cell configuration. This time was necessary to achieve equilibration of the indicator over the dendritic segment of recording (Fig. S2*a* in the Supporting Material). To attain a good signal-to-noise ratio (S/N), fluorescence was averaged over 16-64 trials as specified in each figure legend. Individual trials were saved in separate files and averaged offline. In this way, series of trials where the kinetics of the action potential changed during the sequence were discarded. The $\Delta F/F_0$ signal was calculated without subtraction of the autofluorescence background. The dendritic fluorescence in cells loaded with 1 mM OG5N 25 minutes after establishing the whole-cell configuration decreased with the distance from the soma, as shown in Fig.S2*b* in the Supporting Material. In particular, in the first 100 µm apical segment, dendritic fluorescence was always >3 times larger than autofluorescence estimated in large adjacent regions with a variability of ~15% from cell to cell at the same distance from the soma. This test shows that the contribution of autofluorescence was not critical for the empirical estimates of the Ca^{2+} currents in the proximal apical dendritic regions obtained with the two calibration procedures.

Fluorescence averages were also corrected for bleaching using trials without signal. To achieve a good S/N in the $d(\Delta F/F_0)/dt$ signal, we applied a Savitzky-Golay filter (16) to the $\Delta F/F_0$ signal before differentiation. The filter was implemented by the "smooth" function in the Matlab "Curve Fitting Toolbox". In all data reported here, the OG5N-$\Delta F/F_0$ signal was smoothed using a filter window of 20-30 samples. This filter did not produce any temporal distortion. The Savitzky-Golay filter proved to be the best algorithm to improve the S/N of the $d(\Delta F/F_0)/dt$ signal as described in Fig. S3 in the Supporting Material. Its implementation, however, required signal oversampling which motivated our choice to record fluorescence at the highest possible rate of the camera (20 kHz).

The JPW1114-$\Delta F/F_0$ signal was always calibrated in terms of V_m change on an absolute scale using a previously demonstrated protocol, based on wide-field photorelease of L-glutamate from the caged compound 4-methoxy-7-nitroindolinyl-caged-L-glutamate (MNI-glutamate) (15). Briefly, a calibration of the JPW1114-$\Delta F/F_0$ signal can be done if an electrical signal of known amplitude is available at all recordings sites (12,17). In many neuronal types, activation of a large portion of ionotropic glutamate receptor makes them the dominant conductance and the resulting V_m will be 0 mV in all the illuminated area. Thus, by activation of >50% of the AMPA receptors with glutamate uncaging starting from the resting V_m, we were able to calibrate the JPW1114-$\Delta F/F_0$ signal that corresponded to a change of V_m from the resting V_m to 0 mV.

RESULTS

Low-affinity Ca^{2+} indicators are capable of tracking fast Ca^{2+} currents

The straightforward strategy to test whether I_{Ca} can be derived from a $\Delta F/F_0$ Ca^{2+} signal is to compare the kinetics of $\Delta F/F_0$ signal with that of the I_{Ca} integral ($\int I_{Ca}$). To this purpose, we performed patch clamp recordings from CA1 hippocampal pyramidal neurons in slices of the mouse brain filled with a Ca^{2+} indicator, using an imaging system capable of recording at the frame rate of 20 kHz. We measured I_{Ca} evoked by depolarising pulses from -70 mV to -10 mV in the presence of Na^+ and K^+ channels blockers (see Materials and Methods). With the Ca^{2+} indicator in the patched pipette at 1 mM concentration, we simultaneously recorded $\Delta F/F_0$ from the initial 60 µm apical dendritic segment (Fig. 1*a*). Thus, under these pharmacological conditions, the voltage step depolarised this proximal dendritic region to ~-10 mV for the first 4 ms, a time interval sufficient to explore the fast kinetics of the Ca^{2+} influx (see Fig.S4 in the Supporting Material).

The rate of the dye-Ca^{2+} reaction depends on the affinity (K_D) of the indicator. In that respect, low affinity indicators (K_D > 10 µM) can equilibrate in hundreds of µs (18). Thus, in these experiments, we performed a proof-of-principle test on the high-affinity indicator Oregon Green 488 BAPTA-1 (OGB1, K_D = 206 nM (19)) and on the low-affinity indicator Oregon Green 488 BAPTA-5N (OG5N, K_D = 35-46 µM (8,9)). Fig. 1*b* shows two representative examples of $\Delta F/F_0$ kinetics and of the associated $\int I_{Ca}$ where the two curves were normalised to 1 over the first 4 ms. The $\int I_{Ca}$ curve matched the $\Delta F/F_0$ curve with OG5N, but not with OGB1. To quantify the match between the two curves for the two indicators we computed the area of their difference (S), which was positive for OGB1 and nearly 0 for OG5N (Fig. 1*c*). In two groups of cells, the area of the difference between $\int I_{Ca}$ and $\Delta F/F_0$ was 0.19 ± 0.03 (N = 5 cells) for OGB1, significantly different ($p<0.01$, two-population t-test) from the values obtained for OG5N (0.01 ± 0.02, N = 12). Since OG5N-$\Delta F/F_0$ is proportional to the associated $\int I_{Ca}$, then its derivative must be also proportional to I_{Ca}. In the representative example of Fig. 1*d*, the $d(\Delta F/F_0)/dt$ was calculated after smoothing the $\Delta F/F_0$ signal using a Savitzky-Golay filter (16) (Fig. 1*e*). In conclusion, we demonstrated that the low-affinity indicator OG5N is adequate for tracking in time I_{Ca}.

Extraction of local Ca^{2+} current volume densities from Ca^{2+} fluorescence changes

Differentiation of the OG5N-$\Delta F/F_0$ signal may therefore provide a signal with the same kinetics of I_{Ca} allowing local currents to be measured regionally during a physiological change of V_m. This situation, however, applies only if two additional conditions are met. First, binding to endogenous Ca^{2+} buffers that are slower than OG5N and Ca^{2+} extrusion should be negligible during the entire I_{Ca}, since these two mechanisms decay $\Delta F/F_0$, producing a negative component of $d\Delta F/F_0/dt$. Second, Ca^{2+} release from stores should not contribute to $[Ca^{2+}]_{TOT}$ since this would distort the rise of $\Delta F/F_0$ with respect to the Ca^{2+} influx through the plasma membrane. Fig. 2*a* shows an example of $\Delta F/F_0$ associated with an action potential from the most proximal dendritic segment (0-60 µm from the soma) obtained with OG5N. The $\Delta F/F_0$ onset occurred before the action potential peak and its slope was nearly zero for a few milliseconds after the peak. According to the time course of $\Delta F/F_0$, $d\Delta F/F_0/dt$ reaches the peak at the time of $\Delta F/F_0$ maximal slope and returns to zero. We then re-patched the cell with additional 40 µM BAPTA, which is a high affinity buffer and has slower kinetics compared to OG5N. Thus, BAPTA mimics the presence of an endogenous Ca^{2+} buffer that would be capable of distorting the $d\Delta F/F_0/dt$.

After addition of BAPTA, the $\Delta F/F_0$ decayed more rapidly after the peak, introducing a small negative component to $d\Delta F/F_0/dt$ (Fig. 2*a*). This observation shows that a flat $\Delta F/F_0$ slope after the peak is the indication that both binding to slow endogenous Ca^{2+} buffers and Ca^{2+} extrusion occur less rapidly than Ca^{2+} influx. To exclude Ca^{2+} release from stores during the action potential, we blocked ryanodine receptors with 200 µM ryanodine (20), inositol triphosphate ($InsP_3$) receptors with 100 µg/mL heparine (21), and phospholipase-C and $InsP_3$ formation with 5 µM U73122 (22). The representative cell of Fig. 2*b* was first patched with the control internal solution and, sequentially, with inhibitors of Ca^{2+} release from stores. These had no effect on $\Delta F/F_0$ and on its derivative. This result was consistent in the four cells tested, indicating that Ca^{2+} release from stores doesn't occur during the action potential.

The previous result demonstrates that the OG5N-$\Delta F/F_0$ signal associated with an action potential is exclusively due to Ca^{2+} influx through the plasma membrane. It follows that the $d\Delta F/F_0/dt$ signal can be, in principle, converted into a "I_{Ca} volume density" (I_{Ca}/V) by estimating the $[Ca^{2+}]_{TOT}$ corresponding to a given OG5N-$\Delta F/F_0$ signal. An accurate estimate of I_{Ca}/V in the initial apical dendritic segment was obtained using two independent procedures. In the first procedure, we filled eight cells with a solution also containing 300 µM NP-EGTA (23) and 150 µM $CaCl_2$. NP-EGTA is a photolabile chelator that selectively binds Ca^{2+} with high affinity and releases it rapidly, upon photolysis, in irreversible manner. Under these conditions, a depolarisation from -70 to -10 mV produced a persistent OG5N-

$\Delta F/F_0$ signal >20% in the 80 µm most proximal dendrite (Fig. 3*a*) while a further depolarisation step of +50 mV produced an additional OG5N-$\Delta F/F_0$ >20% (Fig. 3*b*). Since the K_D of NP-EGTA before photolysis is 80 nM (23) and the K_D of OG5N is 35 µM (23), the large and persistent OG5N-$\Delta F/F_0$ increase from -70 to -10 mV indicates that all NP-EGTA is bound to Ca^{2+} at -10 mV. The further larger increase of OG5N-$\Delta F/F_0$ from -10 to +40 mV demonstrates that OG5N is still not saturated at -10 mV. While V_m = -10 mV, 300 µM Ca^{2+} is available for uncaging and a sequence of pulses will progressively release Ca^{2+} until all NP-EGTA is photolysed, i.e. until the whole 300 µM Ca^{2+} is released. Thus, we performed the calibration by applying a sequence of 16 UV pulses (20 ms) and by measuring the OG5N-$\Delta F/F_0$ signal every 5s. The Ca^{2+} released at the pulse *k* follows the geometric progression (24)

$$[\mathrm{Ca}^{2+}]_{\mathrm{TOT}}(k) = \alpha \cdot (300\ \mu M - \sum_{j=0}^{k-1}[\mathrm{Ca}^{2+}]_{\mathrm{TOT}}(j)) \qquad (2)$$

where α is the photolytic conversion per UV pulse. In the cell of Fig. 3*a*, an OG5N-$\Delta F/F_0$ signal of 3.8% corresponded to a $[Ca^{2+}]_{TOT}$ = 93 µM (Fig. 3*c*). The $[Ca^{2+}]_{TOT}$ associated with an action potential was converted into a charge-to-volume ratio (Q/V) using the equation:

$$Q/V = \frac{[Ca^{2+}]_{TOT} \cdot 2e \cdot N_A}{dm^3} \qquad (3)$$

where *e* is the fundamental charge, dm is the decimetre unit and N_A is the Avogadro number (Fig. 3*d*). The smoothed signal was differentiated and expressed as I_{Ca}/V. The current was obtained converting $[Ca^{2+}]_{TOT}$ = 1 µM to an equivalent charge volume density of $1.9297 \cdot 10^{-4}$pC/µm^3. Assuming a uniform conversion factor for the sites included in the calibrating region (most proximal 80 µm dendrite), I_{Ca}/V could be estimated (Fig. 3*e*). In the more distal regions, the $d\Delta F/F_0/dt$ signal has the same kinetics of I_{Ca}, but is not calibrated. In the eight cells analysed in this way, the OG5N-$\Delta F/F_0$ signal of 1% corresponded to a $[Ca^{2+}]_{TOT}$ of 20 ± 3 µM.

In the second procedure, applied to six cells, we sequentially patched the neuron first with 1 mM OG5N in the pipette and later with additional 40 µM of the high-affinity chelator BAPTA. As expected by equation 1, addition of the higher affinity chelator BAPTA, which is slower than OG5N in equilibrating, has negligible effect on the fast peak of the OG5N-$\Delta F/F_0$ signal (Fig. 2*a*). However, BAPTA sequestrates Ca^{2+} both from OG5N and from the endogenous buffer during its slower equilibration, changing the decay of the OG5N-$\Delta F/F_0$ signal. If BAPTA is saturated, the difference between the OG5N-$\Delta F/F_0$ signal before and after addition of BAPTA must correspond to a $[Ca^{2+}]_{TOT}$ equal to the BAPTA concentration. We investigated the OG5N-$\Delta F/F_0$ signal associated with four action potentials elicited at 5 ms interval in control conditions and after re-patching the cell with the solution containing BAPTA, as shown in the cell of Fig. 4*a*. The OG5N-$\Delta F/F_0$ peak associated with the first action potential had nearly the same peak in control solution and with BAPTA, but the OG5N-$\Delta F/F_0$ peak associated with the next action potentials was larger in control solution and the difference in the OG5N-$\Delta F/F_0$ peaks associated with the third and fourth action potential was nearly the same. We concluded that the difference between OG5N-$\Delta F/F_0$ signals with the two solutions, after the third action potential, corresponded to 40 µM Ca^{2+}. We used this difference for the calibration of I_{Ca} /V at the proximal dendrite (Fig. 4*b*). In the six cells calibrated with sequential patch with BAPTA, a OG5N-$\Delta F/F_0$ signal of 1% corresponded to a $[Ca^{2+}]_{TOT}$ of 22 ± 9 µM, similar to what was obtained using the first procedure (Fig. 4*c*). Given these similar results obtained with two different procedures, a standard calibration of OG5N-$\Delta F/F_0$ = 1% corresponding to·$[Ca^{2+}]_{TOT}$ = 20 µM was applied in the proximal dendrite.

Use of optical Ca^{2+} current measurements to study T-type channels

To assess the capability of our novel approach to study the behaviour of native channels under physiological activity, we investigated the voltage-dependence of the I_{Ca}/V associated with action potentials. To this aim, we simultaneously monitored V_m optically with the

voltage-sensitive dye JPW1114 (13). Initially, we measured I_{Ca}/V and V_m associated with an action potential in the proximal apical dendritic segment (Fig. 5*a*). I_{Ca}/V and V_m were measured under two conditions: for an action potential starting at V_m = -60 mV and for an action potential starting at V_m = -80 mV (Fig. 5*b*). When the action potential started at V_m = -80 mV, I_{Ca}/V was larger and started at a more hyperpolarised V_m , indicated as V_m^0 in Fig. 5*c*. This result, consistent in all the six cells tested (Fig. 5*d*), suggested that at V_m = -60 mV I_{Ca} was mediated by different types of high voltage-activated Ca^{2+} channels expressed in this neuronal type (25), whereas I_{Ca}/V starting at V_m = -80 mV contained a contribution of T-type voltage-gated Ca^{2+} channels (26). To confirm this hypothesis, we tested the combined effect of the specific T-type channel blockers (1*S*,2*S*)-2-[2-[[3-(1*H*-Benzimidazol-2-yl)propyl]methylamino]ethyl]-6-fluoro-1,2,3,4-tetrahydro-1-(1-methylethyl)-2-naphthalenyl-cyclopropanecarboxylate-dihydrochloride (NNC, 30 µM) (27) and 3,5-dichloro-*N*-[[(1α,5α,6-exo,6α)-3-(3,3-dimethylbutyl)-3-azabicyclo[3.1.0]hex-6-yl]methyl]-benzamide-hydrochloride (ML218, 5 µM) (28) and of the non-specific voltage-gated Ca^{2+} channel blocker $CdCl_2$ (100 µM) in separate I_{Ca}/V recordings (Fig. 5*e,f*).

As shown in Fig. 5*f,g*, T-type channel blockers inhibit the I_{Ca}/V associated with an action potential starting at V_m = -80 mV, but not the I_{Ca}/V associated with an action potential starting at V_m = -60 mV. This result was consistent in all the cells tested (Fig. 5*h*). In seven cells, the mean ± SD of I_{Ca}/V after addition of NNC+ML218, normalised to I_{Ca}/V in control conditions, was 0.96 ± 0.04 at V_m = -60 mV and 0.77 ± 0.05 at V_m = -80 mV. To further test the efficacy and selectivity of these two relatively new molecules in our preparation, we performed a series of voltage clamp recordings, measuring both the somatic I_{Ca} and the proximal dendritic I_{Ca}/V associated with 16 ms voltage steps either from -80 mV to -20 mV or from -60 mV to 0 mV (Fig. 6*a*). We performed these two recordings first in control conditions and then after addition of NNC and ML218. In this way, we measured, for the two voltage steps, the high-voltage activated Ca^{2+} channels mediated component of the somatic I_{Ca} and of the dendritic I_{Ca}/V both blocked by further addition of 100 µM $CdCl_2$, that at this concentration did not bind to the indicator intracellularly. From these measurements, we extracted the T-type channel component of the electrode and optical I_{Ca} by subtracting the signals in the presence of the T-type channel blockers from the control signals (Fig. 6b). A relevant T-type channel-mediated component of the I_{Ca} was present only when the initial V_m was -80 mV, because, at this initial V_m, these channels recover from inactivation. In the six cells tested, the T-type current and the optically measured T-type current volume density associated with a -80 mV to -20 mV pulse were 1.18 ± 0.48 nA and 1.31 ± 0.60 pA/µm^3, respectively. The same signals associated with a step from -60 mV to 0 mV were 0.25 ± 0.12 and 0.30 ± 0.18 pA/µm^3, respectively.

In conclusion, we confirm by using our optical recordings that T-type Ca^{2+} channels are inactivated at V_m = -60 mV and that recovery from inactivation by setting the initial V_m = -80 mV permits their activation during the action potential.

Next, we investigated from a longer apical dendritic segment the I_{Ca}/V starting from the resting V_m (typically between -70 mV and -60 mV), uniform along the apical dendrite (29). In these experiments, the protocol consisted of two action potentials elicited at 5 ms time interval (Fig. 7*a*).

The second action potential was characterised by a decrease in amplitude (Fig. 7*b*), characteristic of CA1 hippocampal pyramidal neurons (30). This decrease was reflected by a concomitant decrease of the second I_{Ca}/V. Interestingly, the time of the I_{Ca}/V onset in the distal region corresponded to a more hyperpolarised V_m for the second action potential (Fig. 7*c*), a result consistent in all 5 cells tested (Fig. 7*d*). This unexpected result suggested that an additional T-type channel contribution, independent of the initial V_m, was associated with the second action potential. To explore this hypothesis we tested the delay in the peak of I_{Ca}/V (Δt) produced by the addition of NNC and ML218 (Fig. 7*e,f*). T-type channel blockers delayed the I_{Ca}/V associated with the second action potential, but not that associated with the first action potential, as shown in Fig. 7*f*. In the six cells tested (Fig. 7*g*), the delay

produced by NNC and ML218 to the second I_{Ca}/V was 0.52 ± 0.09 ms proximally and 0.59 ± 0.09 ms distally. These values were significantly different ($p<0.01$, two-population t-test) from the delays produced by NNC and ML218 to the I_{Ca}/V associated with the first action potential (0.11 ± 0.02 ms proximally and 0.08 ± 0.02 ms distally). These results show that activation and recovery from inactivation of T-type Ca^{2+} channels during action potentials can be quantitatively investigated together with the V_m and from multiple dendritic sites, using our novel approach. Equivalent information cannot be achieved with other existent methods.

DISCUSSION

In this report, we present an original and unique approach that allows the measurement of a local fast Ca^{2+} current from single cells without the constraints of the voltage clamp technique. In particular, the current can be measured during the physiological change of V_m in combination with the synergistic occurrence of other currents. In the single-electrode voltage clamp approach the current measurement is the recording of the total charge flux through the plasma membrane. In contrast, in our method, the measurement consists in the extrapolation of a Ca^{2+} current volume density from the local recording of the concentration of the Ca^{2+} bound to the dye.

The idea of using Ca^{2+} imaging to extract Ca^{2+} flux and to explore Ca^{2+} channels is historical and was extensively utilised in muscle research (31). Using Ca^{2+} dynamics modelling and Ca^{2+} unitary events, namely Ca^{2+} sparks, Ca^{2+} currents through membranes of intracellular stores were estimated in skeletal muscles (32,33) and cardiac muscles (34). More recently, Ca^{2+} currents through muscular intracellular membranes were estimated using the “total” fluorescence increase (or signal mass) (35,36). These methods are based on the utilisation of the high-affinity indicators Fluo-3 and Fluo-4, which are characterised by a large dynamic range resulting in large changes of fluorescence upon Ca^{2+} increase. Our novel approach utilises the low-affinity indicator OG5N, which allows reconstruction of the kinetics of the current at higher temporal resolution. OG5N is used at relatively high concentration (1 mM). Assuming K_D = 35 µM for OG5N, the buffering capacity of the indicator is smaller than the estimated endogenous buffering capacity of the CA1 hippocampal pyramidal neuron dendrite (37). In contrast to the methods developed in the muscle, our method allows investigating Ca^{2+} channels expressed in the plasma membrane in combination with patch clamp recordings and V_m imaging to analyse the voltage dependence of the channels. In this respect, the test that Ca^{2+} release from stores is negligible during Ca^{2+} influx is always crucial since this possibility may occur during neuronal firing activity (38). Finally, the combined optical measurement of the action potential is also useful to test whether the measurement is locally affected by photodamage (13).

The quantitative measurement of I_{Ca}/V described here is only the first step towards the use of this method to monitor the activated Ca^{2+} channels distribution over the cell since this task will require additional information on the I_{Ca} surface density. The I_{Ca} from a dendritic branch can be simply extracted using the cylindrical approximation of the dendrite. For instance, the current from a dendritic segment of 10 µm with I_{Ca}/V = 10 pA/µm^3 and a radius of 1 µm will be 31.4 pA. The accurate estimate of the radius, however, cannot be obtained using standard fluorescence microscopy. Thus, a more precise radius measurement can be achieved by confocal microscopy, for instance by taking an image of the dendrite using a spinning disk.

Among the several important applications in which this technique will be relevant, it is worth mentioning the study of activity-dependent modulation of Ca^{2+} channels during physiological activity, the study of functional changes associated with Ca^{2+} channels mutations and pathological conditions, and the implementation of neuron computational

models based on optically-measured local Ca^{2+} currents. The method is based on the use of a specialised high-speed dual CCD camera but novel and more economical CMOS technology seems to be also suitable for this application (39). Here, to validate the technique, we report an original study of I_{Ca} associated with action potentials recorded at the apical dendrite of CA1 hippocampal pyramidal neurons. Our results show that during an action potential, dendritic high-voltage activated Ca^{2+} channels can be always activated by V_m depolarisation produced by the Na^+ current and are closed by V_m hyperpolarisation produced by the K^+ current. In contrast, the opening of T-type channels depends on the state of the channel before the action potential (40). When the cell is not firing, most T-type Ca^{2+} channels are inactivated unless the initial V_m, is <-80 mV. However, during firing activity, our results suggest that recovery from inactivation may occur independently of the V_m.

CONCLUSION

The present approach should drastically improve our understanding of the physiological function of Ca^{2+} channels by providing the possibility to explore the biophysics of native channels during physiological activity in subcellular loci of the complex neuronal architecture.

ACKNOWLEDGEMENTS

We thank Philippe Moreau for technical help, Jean-Claude Vial for useful discussions and David Ogden and Joseph Gallagher for reading and revising the manuscript. All experiments were performed at the “Laboratoire Interdisciplinaire de Physique” (LiPhy) at the Joseph Fourier University. This work was supported by the *Agence Nationale de la Recherche* (Grant *Voltimagmicro*, program *Emergence-10*, Labex *Ion Channels Science and Therapeutics:* program number ANR-11-LABX-0015 and National Infrastructure France Life Imaging “Noeud Grenoblois”).

REFERENCES

1. Sakmann, B., and E. Neher. 1986. Patch clamp techniques for studying ionic channels in excitable membranes. *Annu. Rev. Physiol.* 46:455-472.

2. Williams, S.R., and S.J. Mitchell. 2008. Direct measurement of somatic voltage clamp errors in central neurons. *Nat. Neurosci.* 11:790-798.

3. Stuart, G.J., and N. Spruston. 1995. Probing dendritic function with patch pipettes. *Curr. Opin. Neurobiol.* 5:389-394.

4. Tsien, R.Y. 1989. Fluorescent indicators of ion concentrations. *Methods Cell. Biol.* 30:127-156.

5. Canepari, M., and F. Mammano. 1999. Imaging neuronal calcium fluorescence at high spatio-temporal resolution. *J. Neurosci. Meth.* 87:1-11.

6. Kao, J.P., and R.Y. Tsien. 1988. Ca2+ binding kinetics of fura-2 and azo-1 from temperature-jump relaxation measurements. *Biophys. J.* 53:635-639.

7. Sabatini, B.L., and W.G. Regehr. 1998. Optical measurement of presynaptic calcium currents. *Biophys. J.* 74:1549-1563.

8. Canepari, M., and D. Ogden. 2006. Kinetic, pharmacological and activity-dependent separation of two Ca2+ signalling pathways mediated by type 1 metabotropic glutamate receptors in rat Purkinje neurones. *J. Physiol.* 573:65-82.

9. Woods, C.E., D. Novo, M. DiFranco, and J.L. Vergara. 2004. The action potential-evoked sarcoplasmic reticulum calcium release is impaired in mdx mouse muscle fibres. *J. Physiol.* 557:59–75.

10. Antic, S., and D. Zecevic. 1995. Optical signals from neurons with internally applied voltage-sensitive dyes. *J. Neurosci.* 15:1392-1405.

11. Jaafari, N., M. Henson, J. Graham, and M. Canepari. 2013. Economic and simple system to combine single-spot photolysis and whole-field fluorescence imaging. *J. Biomed. Opt.* 18:60505.

12. Canepari, M., K. Vogt, and D. Zecevic. 2008. Combining Voltage and Calcium Imaging from Neuronal Dendrites. *Cell. Mol. Neurobiol.* 28:1079-1093.

13. Canepari, M., Willadt, S., Zecevic, D., and K.E. Vogt. 2010. Imaging Inhibitory Synaptic Potentials Using Voltage Sensitive Dyes. *Biophys. J.* 98:2032-2040.

14. Vogt, K.E., S. Gerharz, J. Graham, and M. Canepari. 2011. High-resolution simultaneous voltage and Ca2+ imaging. *J. Physiol.* 589:489-494.

15. Vogt, K.E., S. Gerharz, J. Graham, and M. Canepari. 2011. Combining membrane potential imaging with L-glutamate or GABA photorelease. *PLoS ONE* 6:e24911.

16. Savitzky, A., and M.J.E. Golay. 1964. Smoothing and Differentiation of Data by Simplified Least Squares Procedures. *Anal. Chem.* 36:1627-1639.

17. Canepari, M. and K.E., Vogt KE. 2008. Dendritic spike saturation of endogenous calcium buffer and induction of postsynaptic cerebellar LTP. *PLoS ONE* 3: e4011.

18. Baylor, S.M. and S. Hollingworth. 2011. Calcium indicators and calcium signalling in skeletal muscle fibres during excitation-contraction coupling. *Prog. Biophys. Mol. Biol.* 105: 162-179.

19. Sabatini, B.L., T.G. Oertner, and K. Svoboda. 2002. The life cycle of Ca(2+) ions in dendritic spines. *Neuron* 33:439–452.

20. Sutko, J.L., J.A. Airey, W. Welch, and L. Ruest. 1997. The pharmacology of ryanodine and related compounds. *Pharmacol. Rev.* 49:53-98.

21. Ghosh, T.K., P.S. Eis, J.M. Mullaney JM, C.L. Ebert, and D.L. Gill. 1988. Competitive, reversible, and potent antagonism of inositol 1,4,5-trisphosphate-activated calcium release by heparin. *J. Biol. Chem.* 263:11075-11079.

22. Bleasdale, J.E., N.R. Thakur, R.S. Gremban, G.L. Bundy, F.A. Fitzpatrick, R.J. Smith, and S. Bunting. 1990. Selective inhibition of receptor-coupled phospholipase C-dependent processes in human platelets and polymorphonuclear neutrophils. *J. Pharmacol. Exp. Ther. 255*:756-768.

23. Ellis-Davies, G.C., and J.H. Kaplan. 1994. Nitrophenyl-EGTA, a photolabile chelator that selectively binds Ca2+ with high affinity and releases it rapidly upon photolysis. *Proc. Natl. Acad. Sci. USA* 91**:**187-191.

24. Canepari, M., Nelson, L., Papageorgiou, G., Corrie, J.E.T., and D. Ogden. 2001. Photochemical and pharmacological evaluation of 7-nitroindolinyl-and 4-methoxy-7-nitroindolinyl-amino acids as novel, fast caged neurotransmitters. *J. Neurosci. Meth.* 112:29-42.

25. Kavalali, E.T., M. Zhuo, H. Bito, and R.W. Tsien. 1997. Dendritic Ca2+ channels characterized by recordings from isolated hippocampal dendritic segments. *Neuron* 18:651-663.

26. Cueni, L., M. Canepari, J.L. Adelman, and A. Lüthi. 2009. Ca2+ signaling by T-type Ca2+ channels in neurons. *Pflugers Arch.* 457:1161–1172.

27. Huang, L., B.M. Keyser, T.M. Tagmose, J.B. Hansen, J.T. Taylor, H. Zhuang, M. Zhang, D.S. Ragsdale, and M. Li. 2004. NNC 55-0396 [(1*S*,2*S*)-2-(2-(*N*-[(3-benzimidazol-2-yl)propyl]-*N*-methylamino)ethyl)-6-fluoro-1,2,3,4-tetrahydro-1-isopropyl-2-naphtyl cyclopropanecarboxylate dihydrochloride]: A new selective inhibitor of T-type calcium channels. *J. Pharmacol. Exp. Ther.* 309:193-199.

28. Xiang Z., A.D. Thompson, J.T. Brogan, M.L. Schulte, B.J. Melancon, D. Mi, L.M. Lewis, B. Zou, L. Yang, R. Morrison, T. Santomango, F. Byers, K. Brewer, J.S. Aldrich, H. Yu, E.S. Dawson, M. Li, O. McManus, C.K. Jones, J.S. Daniels, C.R. Hopkins, X.S. Xie, P.J. Conn, C.D. Weaver, and C.W. Lindsley. 2011. The discovery and characterization of ML218: A novel, centrally active T-type calcium channel inhibitor with robust effects in STN neurons and in a rodent model of Parkinson's disease. *ACS Chem. Neurosci.* 2:730-742.

29. Gasparini, S., and J.C. Magee. 2002. Phosphorylation-dependent differences in the activation properties of distal and proximal dendritic Na+ channels in rat CA1 hippocampal neurons. *J. Physiol.* 541:665-672.

30. Andreasen, M., and J.D. Lambert. 1995. Regenerative properties of pyramidal cell dendrites in area CA1 of the rat hippocampus. *J. Physiol.* 483:421-441.

31. Wang, S.Q., Wei, C., Zhao, G., Brochet, D.X., Shen, J., Song, L.S., Wang, W., Yang, D., and Cheng, H. 2004 Imaging microdomain Ca2+ in muscle cells. *Circ. Res.* 94: 1011-1022.

32. Klein, M.G., Cheng, H., Santana, L.F., Jiang, Y.H., Lederer, W.J., and Schneider, M.F. 1995. Two mechanisms of quantized calcium release in skeletal muscle. *Nature* 379: 455-458.

33. Tsugorka, A., Ríos, E., and Blatter, L.A. 1996. Imaging elementary events of calcium release in skeletal muscle cells. *Science* 269: 1723-1726.

34. Shkryl, V.M., Blatter, L.A., and Ríos, E. 2012. Properties of Ca2+ sparks revealed by four-dimensional confocal imaging of cardiac muscle. *J. Gen. Physiol.* 139: 189-207.

35. Zhuge, R., Fogarty, K.E., Tuft, R.A., Lifshitz, L.M., Sayar, K., Walsh, J.V. Jr. 2000 Dynamics of signaling between Ca(2+) sparks and Ca(2+)- activated K(+) channels studied with a novel image-based method for direct intracellular measurement of ryanodine receptor Ca(2+) current. *J. Gen. Physiol.* 116: 845-864.

36. Zou, H., Lifshitz, L.M., Tuft, R.A., Fogarty, K.E., and Singer J.J. 2004. Using total fluorescence increase (signal mass) to determine the Ca2+ current underlying localized Ca2+ events. *J. Gen. Physiol.* 124: 259-272.

37. Maravall, M., Mainen, Z.F., Sabatini, B.L., and Svoboda, K. 2000. Estimating intracellular calcium concentrations and buffering without wavelength ratioing. *Biophys. J.* 78: 2655-2667.

38. Sandler, V.M. and Barbara, J.G. 1999. Calcium-induced calcium release contributes to action potential-evoked calcium transients inhippocampal CA1 pyramidal neurons. *J. Neurosci.* 19: 4325-4336.

39. Davies, R., Graham, J., and Canepari, M. 2013. Light Sources and Cameras for Standard in Vitro Membrane Potential and High-Speed Ion Imaging. *J. Microsc.* 251: 5-13.

40. Kuo, C.C., and S. Yang. 2001. Recovery from inactivation of T-type Ca2+ channels in rat thalamic neurons. *J. Neurosci.* 21:1884-1892.

FIGURE LEGEND

FIGURE 1 The change of fluorescence of OG5N matches the integral of a Ca^{2+} current. (***a***) voltage clamp protocol on a CA1 hippocampal pyramidal neuron (shown in the inset) consisting of two 16 ms voltage pulses from -70 mV, the first to ~-60 mV below the threshold for activation of Ca^{2+} channels and the second to ~20 mV; experiments were performed in the presence of Na^+ and K^+ channels blockers; I_{Ca} (indicated as Ca^{2+} current) was extracted by subtraction of the scaled current associated with the sub-threshold pulse minus the current associated with larger voltage pulse for the period limited by the dotted box; the kinetics of the current were analysed in correlation with that of the $\Delta F/F_0$ signal in the initial 60 µm segment of the apical dendrite (gray trace). (***b***) Two neurons, shown in the insets, filled either with OGB1 or OG5N, with the $\int I_{Ca}$ (black) and Ca^{2+} $\Delta F/F_0$ normalised to their maxima; differences between the two curves ($\int I_{Ca}$-$\Delta F/F_0$) also reported; the surface of this difference (S) is indicated. (***c***) Mean ± SD of S for OGB1 and OG5N; values of S are significantly different (two-population t-test, $p<0.01$). (***d***) Voltage clamp I_{Ca} measurement (average of 16 trials) with OG5N: I_{Ca} measured with the patch electrode (top) and the associated $\Delta F/F_0$ from the initial 60 µm apical dendritic segment (bottom) are shown. (***e***) Filtered $\Delta F/F_0$ ($\Delta F/F_0^*$, top-left) and its derivative (bottom-left); on the right, the $\Delta F/F_0^*$ derivative is superimposed to I_{Ca}.

FIGURE 2 Ca^{2+} sequestration by slow endogenous buffer and Ca^{2+} release from stores are negligible during an action potential. (***a***) Neuron patched first with control solution plus 300 µM EGTA and OG5N and sequentially with additional 40 µM BAPTA; an action potential (top), the associated $\Delta F/F_0$ (middle) and $d\Delta F/F_0/dt$ (bottom) are shown; addition of BAPTA fastens the decay $\Delta F/F_0$ introducing a negative component to $d\Delta F/F_0/dt$; in the BAPTA column the control signal is superimposed in gray; (***b***) Same protocol as in ***a*** with sequential patch first with control solution and later with additional Ca^{2+} release from stores inhibitors (CRSIs); $\Delta F/F_0$ and $d\Delta F/F_0/dt$ do not change after addition of CRSIs; in the CRSIs column the control signal is superimposed in gray. Data were from averages of 32 trials.

FIGURE 3 I_{Ca}/V calibration using NP-EGTA. (***a***) Full-resolution and binned-resolution images of the apical dendrite; *R0*: region of calibration; *R1-R4* additional regions of interest; the calibration does not apply to *R3* and *R4*. (***b***) OG5N-$\Delta F/F_0$ from *R0* associated with a voltage step from -70 mV to -10 mV (top) and another voltage step from -10 mV to +40 mV (bottom). (***c***) $\Delta F/F_0$ (gray) with a peak of 3.8% was associated with photorelease of 93 µM Ca^{2+} from NP-EGTA by fitting the signals of a sequence of 16 pulses to equation 2. (***d***) From the same cell, the $\Delta F/F_0$ associated with an action potential (black) was filtered and differentiated (gray); I_{Ca}/V obtained from $d(\Delta F/F_0/dt)$ using calibration in ***a***; data are from averages of 64 trials. (***e***) Using the calibration in ***a***, I_{Ca}/V from regions *R1-R4* associated with an action potential.

FIGURE 4 Calibration of I_{Ca} /V using BAPTA injection. (***a***) OG5N-$\Delta F/F_0$ signals from the initial 80 µm segment (region *R0*) of the cell shown above associated with trains of 4 action potentials (black trace) at 200 Hz; Recordings were completed under control conditions (1 mM OG5N + 300 µM EGTA) and after re-patching the cell with the same solution, which also contained 40 µM BAPTA; the difference of the two OG5N-$\Delta F/F_0$ signals corresponds to $[Ca^{2+}]_{TOT}$ = 40 µM. (***b***) I_{Ca} /V associated with the train of 4 action potentials (black trace) in control conditions from the regions *R0-R1* (gray traces); the calibration does not apply to *R1*. (***c***) The mean ± SD of the ratios between $[Ca^{2+}]_{TOT}$ and OG5N-$\Delta F/F_0$ obtained with the protocol using NP-EGTA or with the protocol using BAPTA. All data were from averages of 32 trials.

FIGURE 5 Dendritic I_{Ca}/V associated with an action potential at different starting V_m. (***a***) Fluorescence images of a cell filled with OG5N (left image) and JPW1114 (right image); the top and bottom images are at full-resolution and binned-resolution, respectively; the region of interest from where fluorescence was averaged is outlined. (***b***) I_{Ca} /V associated with one action potential starting either at V_m = -60 mV or -80 mV; the V_m recorded optically and with the electrode (black trace) are superimposed. (***c***) I_{Ca}/V superimposed to the action potential in the two cases; the V_m at the current onset (V_m^0) is indicated. (***d***) I_{Ca}/V peak and V_m^0 associated with action potentials starting either at V_m = -60 mV or at -80 mV from 6 cells. (***e***) Neuron filled with OG5N: region of interest outlined. (***f***) I_{Ca}/V associated with action potentials (black trace) starting either at V_m = -60 mV or -80 mV: control conditions, after addition of NNC+ML218 and after addition of $CdCl_2$. (***g***) I_{Ca}/V in the different conditions (illustrated in different colours) superimposed (inhibition by T-type channel blockers of I_{Ca}/V starting at V_m = -80 mV). (***h***) The mean ± SD (N = 7 cells) of I_{Ca}/V with NNC+ML218 normalised to control I_{Ca}/V at V_m = -60 mV and -80 mV; $p<0.01$, two-population t-test. Data were from averages of 32 trials.

FIGURE 6 Pharmacological tests of T-type channel blockers NNC and ML218 in voltage clamp experiments. (***a***) Top: initial dendritic segment of a CA1 hippocampal pyramidal neuron; experiments were performed in the presence of Na^+ and K^+ channels blockers; fluorescence was averaged over the entire region; bottom: I_{Ca} measured with the patch electrode or optically (I_{Ca} /V) associated with depolarising pulses either from -80 mV to -20 mV or from -60 mV to 0 mV in voltage clamp; the recordings were performed in control conditions, in the presence of the T-type channel blockers NNC (30 µM) and ML218 (5 µM) and after further addition of $CdCl_2$ (100 µM) are represented in different colours. (**b**) Electrode and optically recorded T-type currents from -80 mV to -20 mV and from -60 mV to 0 mV obtained by subtracting the currents with NNC and ML218 from the control currents; on the right, the mean ± SD (N = 6 cells) of both electrode and optically recorded T-type currents associated with the two voltage steps were significantly different ($p<0.01$, paired T-test). All data were from averages of 16 trials.

FIGURE 7 Dendritic I_{Ca}/V associated with 2 action potentials at 200 Hz. (***a***) Cell filled with OG5N and JPW1114 dye; proximal (*prox*) and distal (*dist*) regions of interest are outlined. (***b***) Proximal and Distal I_{Ca}/V (gray) associated with two action potentials recorded optically (black) at 5 ms interval starting from resting V_m which was 67 mV in this particular cell. (***c***) I_{Ca}/V superimposed to the two action potentials proximally and distally; the V_m at the current onset (V_m^0) is indicated. (***d***) V_m^0 associated with the two action potentials proximally and distally from 5 cells. (***e***) Neuron filled with OG5N: proximal and distal regions are outlined. (***f***) Proximal and distal I_{Ca}/V (gray) associated with two action potentials (black) at 5 ms interval starting from resting V_m (68 mV); recordings were performed in control conditions and after addition of NNC+ML218. (***g***) I_{Ca}/V in control (gray) and after addition of T-type channel blockers (black); T-type channel blockers delays (Δt) the second I_{Ca}/V with respect to the first I_{Ca}/V. (***h***) The mean ± SD (N = 6 cells) of proximal and distal delay (Δt) produced by addition of T-type channel blockers; the difference of Δt between the first and the second action potential both proximally and distally was significant ($p<0.01$, two-population t-test). Data were from averages of 32 trials.

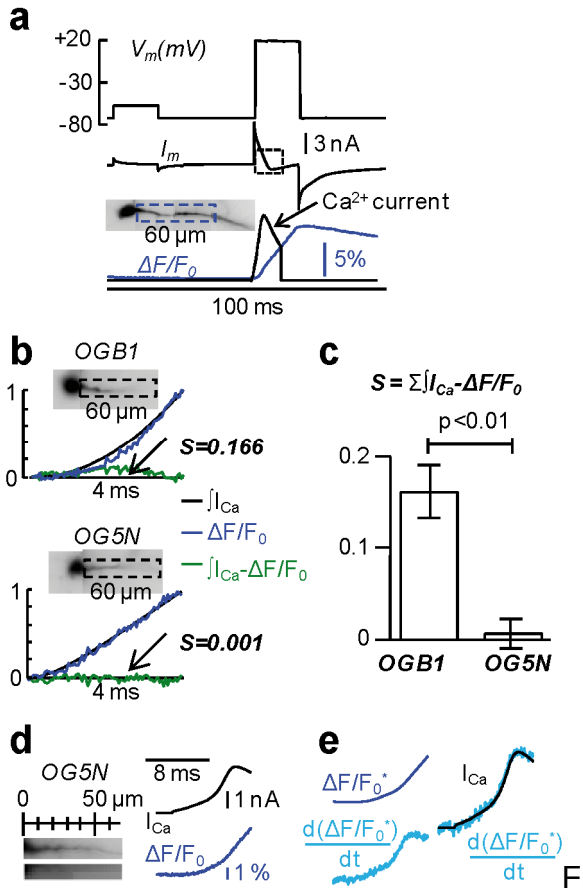

Figure 1

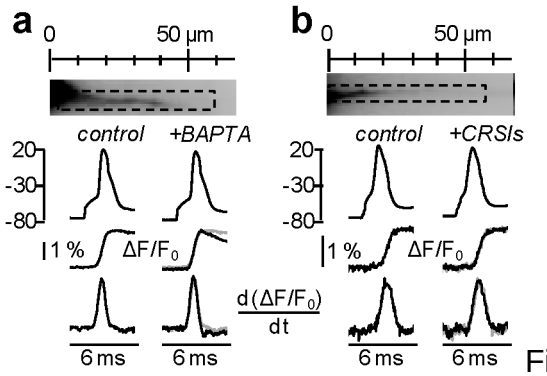

Figure 2

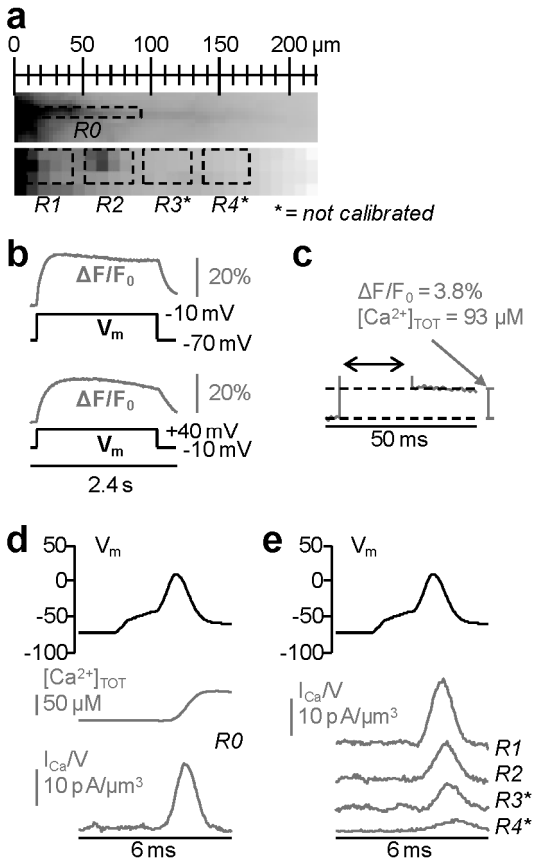

Figure 3

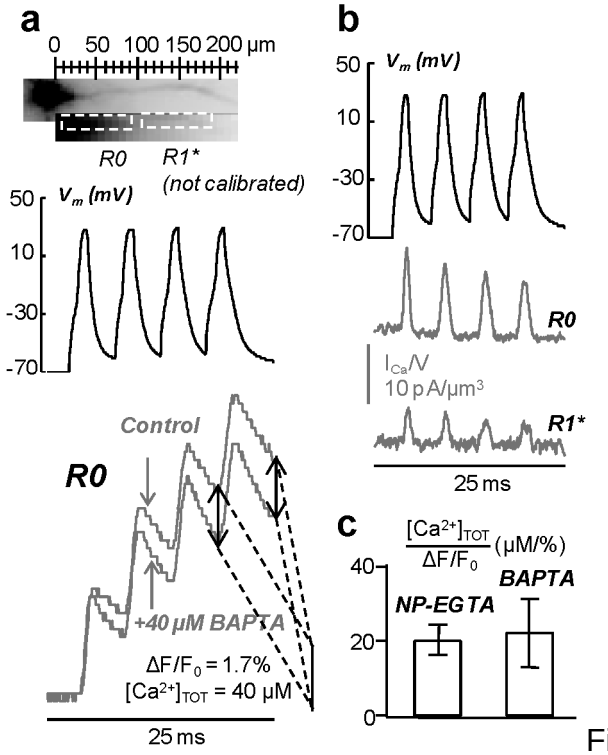

Figure 4

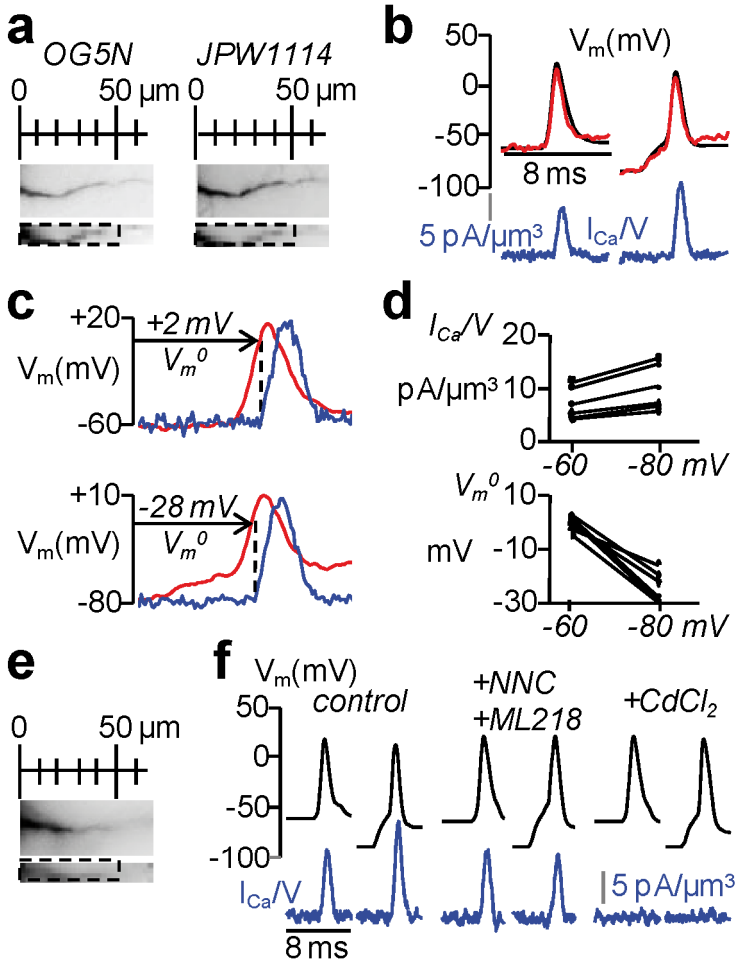
a
OG5N
JPW1114
0
50 µm
0
50 µm
b
50
0
-50
-100
Vm(mV)
8 ms
5 pA/µm³
ICa/V
c
+20
+2 mV
Vm(mV)
Vm0
-60
+10
-28 mV
Vm(mV)
Vm0
-80
d
ICa/V
20
pA/µm³ 10
0
-60
-80 mV
Vm0
10
mV -10
-30
-60
-80 mV
e
0
50 µm
f
Vm(mV)
control
+NNC
+ML218
+CdCl2
50
0
-50
-100
ICa/V
5 pA/µm³
8 ms
g
control
+NNC+ML218
+CdCl2
5 pA/µm³
4 ms
-60 mV
-80 mV
h
ICa(NNC+ML218)
ICa(control)
p<0.01
1.5
1
0.5
0
-60 mV
-80 mV

Figure 5

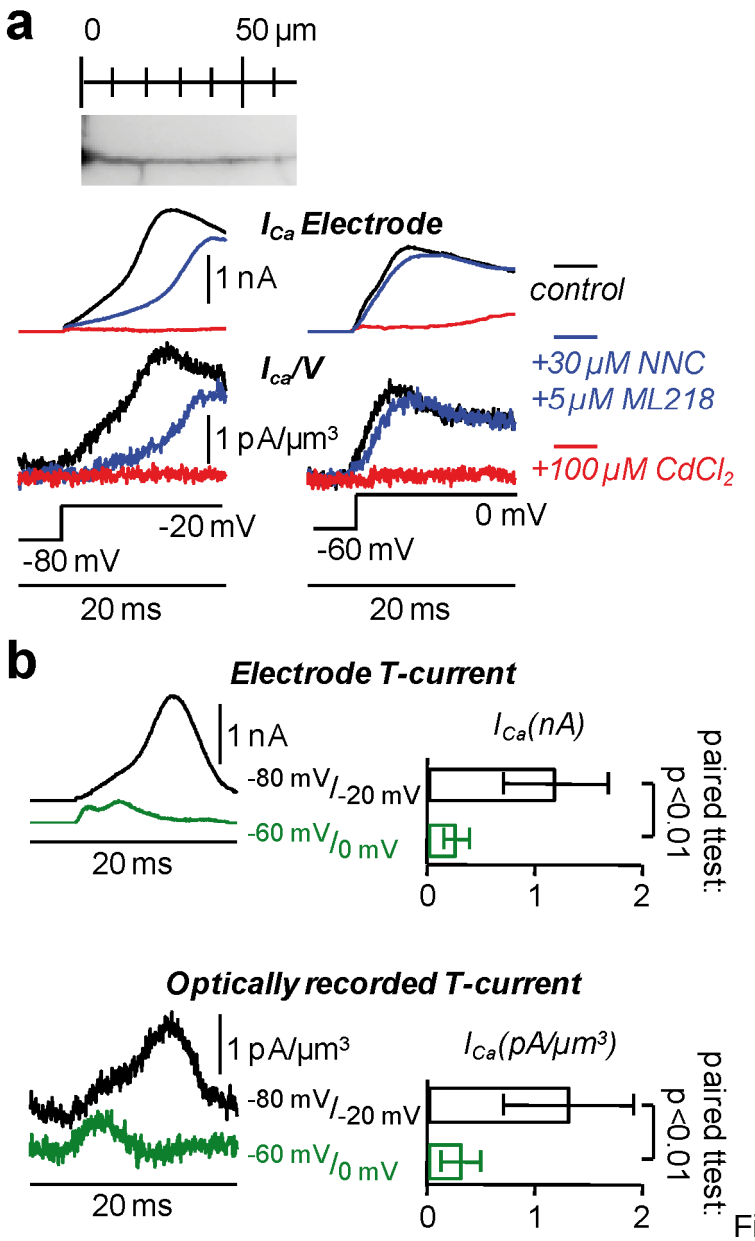
a
0
50 µm
I_{Ca} Electrode
1 nA
control
+30 µM NNC
+5 µM ML218
+100 µM $CdCl_2$
I_{ca}/V
1 pA/µm³
-20 mV
-80 mV
0 mV
-60 mV
20 ms
20 ms
b
Electrode T-current
1 nA
I_{Ca}(nA)
-80 mV/-20 mV
-60 mV/0 mV
20 ms
0
1
2
paired ttest:
p<0.01
Optically recorded T-current
1 pA/µm³
I_{Ca}(pA/µm³)
-80 mV/-20 mV
-60 mV/0 mV
20 ms
0
1
2
paired ttest:
p<0.01

Figure 6

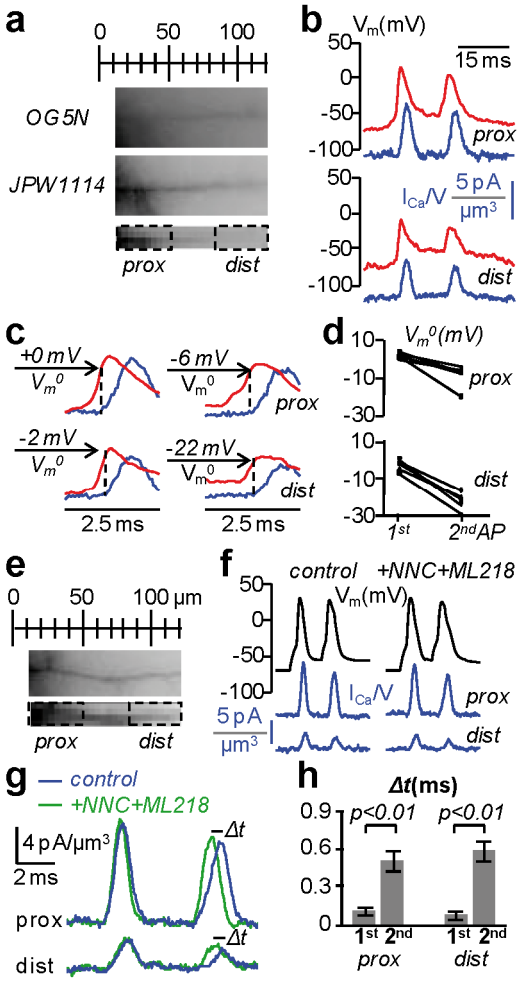
a
0
50
100
OG5N
JPW1114
prox
dist
b
Vm(mV)
50
0
-50
-100
15 ms
prox
ICa/V
5 pA
µm3
dist
c
+0 mV
Vm0
-6 mV
prox
-2 mV
-22 mV
dist
2.5 ms
2.5 ms
d
Vm0(mV)
10
-10
-30
prox
dist
1st
2ndAP
e
0
50
100 µm
prox
dist
f
control
+NNC+ML218
Vm(mV)
ICa/V
prox
5 pA
µm3
dist
g
control
+NNC+ML218
4 pA/µm3
2 ms
−Δt
prox
dist
h
Δt(ms)
0.9
0.6
0.3
0
p<0.01
p<0.01
1st
2nd
prox
dist

Figure 7